ZIF-derived CoS@CN with a hollow cage structure for improved electrochemical nitrate reduction to synthesize ammonia

Yanli Zhang,[a] Jiuqing Xiong,[a] Xuyang Wang,[a] Ming Li,[*a] Shihai Yan,[*a] Bingping Liu[*a]

[a] College of Chemistry and Pharmaceutical Sciences, Qingdao Agricultural University, Qingdao, 266109, China

Corresponding author:

Ming Li, E-mail: liming0414@qau.edu.cn; QAU, Qingdao, 266109, China
Shihai Yan, email: shyan@qau.edu.cn; QAU, Qingdao, 266109, China
Bingping Liu, email: bpliu@qau.edu.cn; QAU, Qingdao, 266109, China

Contents:

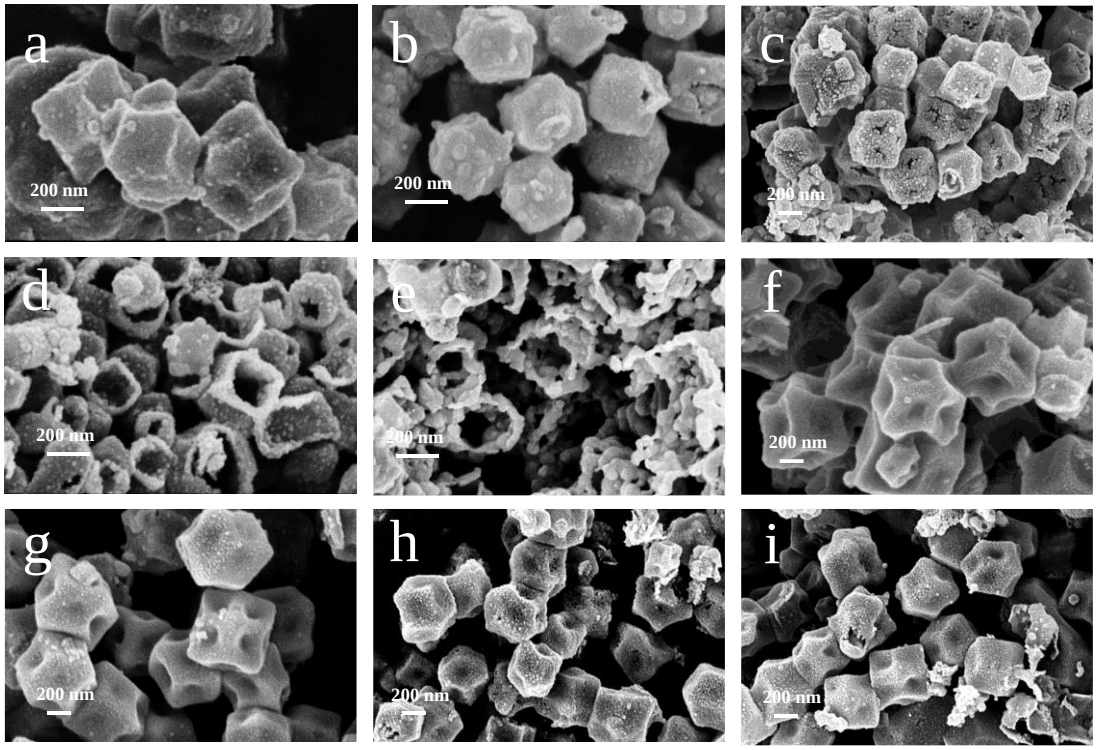

Supplementary Figure 1. SEM of (a) CoS@NC-1, (b) CoS@NC-2, (c) CoS@NC-3, (d) CoS@NC-4, and (e) CoS@NC-5 at 500 ℃, (f) CoS@NC-100, (g) CoS@NC-200, (h) CoS@NC-300, and (i) CoS@NC-400 for 3h.

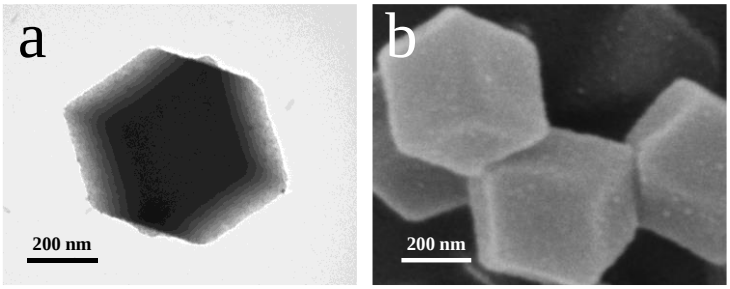

Supplementary Figure 2. (a) TEM and (b) SEM of Co@NC.

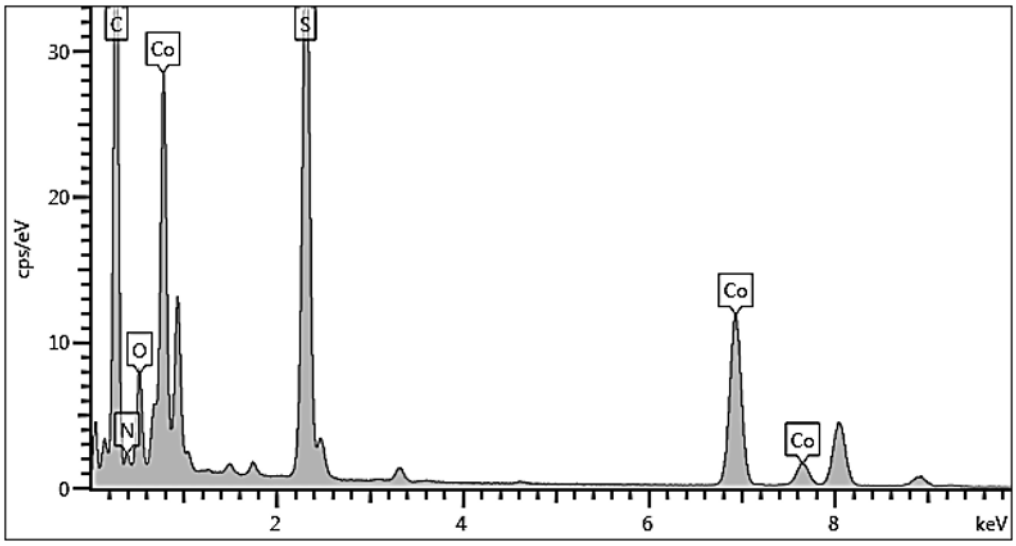

Supplementary Figure 3. The total spectrum of the distribution map in EDS of CoS@CN-300.

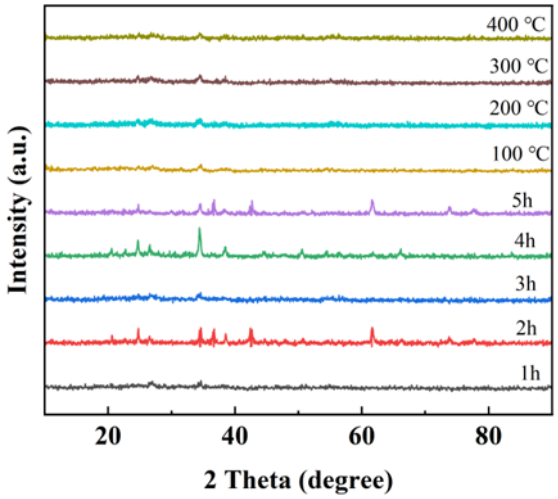

Supplementary Figure 4. XRD patterns of CoS@CN-*x*/*y* (*x* = 1 ~ 5; *y* = 100 ~ 500).

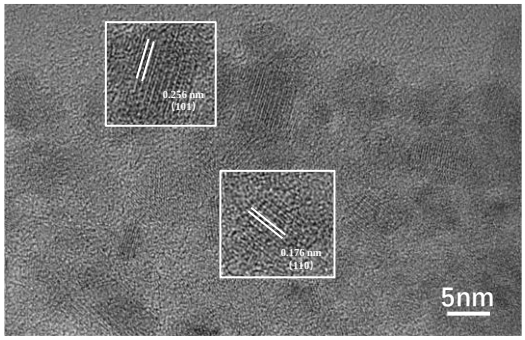

Supplementary Figure 5. The High-Resolution Transmission Electron Microscopy of CoS@CN-300.

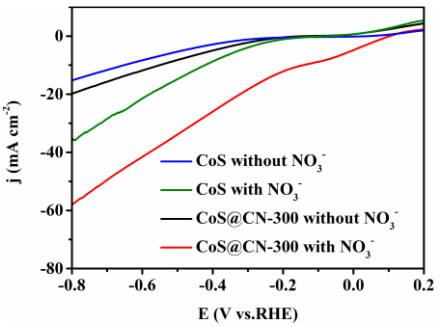

Supplementary Figure 6. LSV of CoS and CoS@CN-300 with and without 0.1 M NO_3^-.

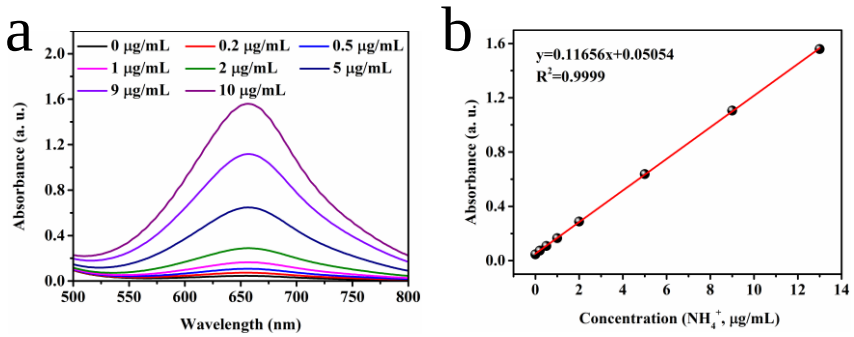

Supplementary Figure 7. (a) UV-vis absorption spectra of various NH_3 concentrations after incubated for 2 h under room temperature and (b) Calibration curve used for estimation of NH_3 concentration.

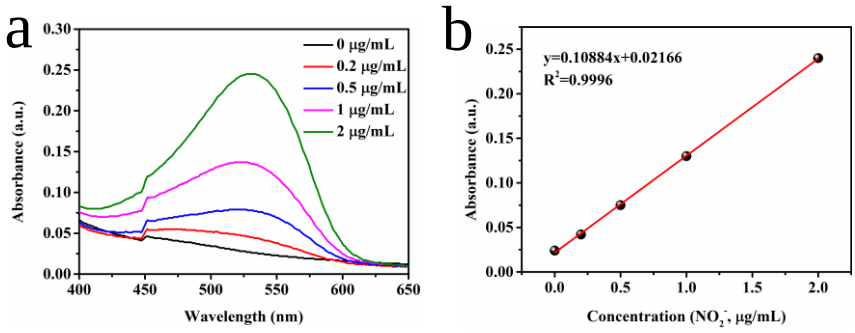

Supplementary Figure 8. (a) UV-vis absorption spectra of various NO_2^- concentrations and (b) Calibration curve used for estimation of NO_2^- concentration.

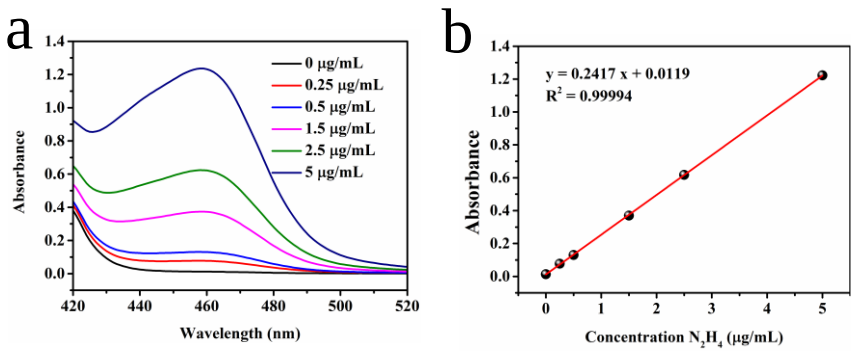

Supplementary Figure 9. (a) UV-vis absorption spectra of various N_2H_4 concentrations and (b) Calibration curve used for estimation of N_2H_4 concentration.

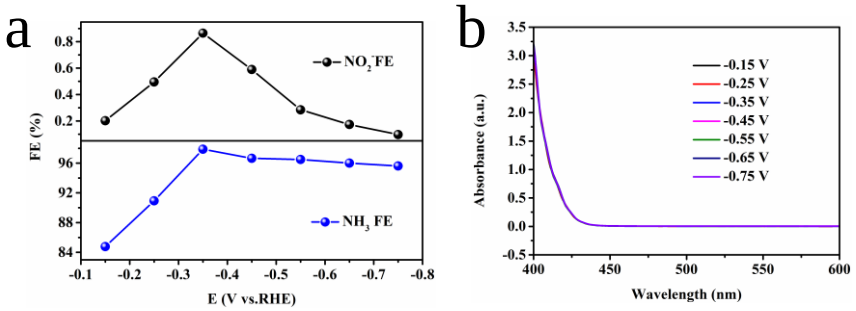

Supplementary Figure 10. The comparison (a) FE of NO_2^- and NH_3. (b) UV-vis absorption spectra of detecting N_2H_4 in eNO_3RR.

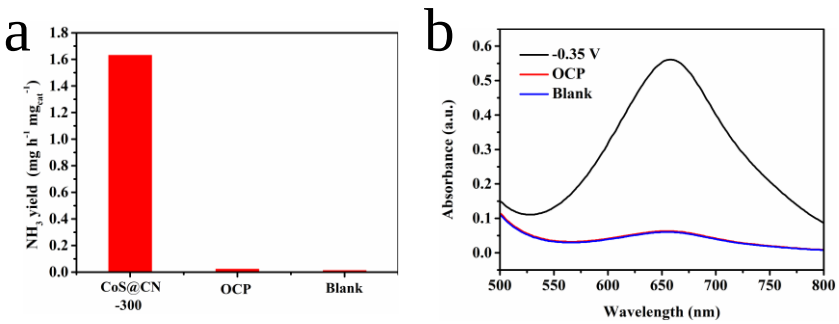

Supplementary Figure 11. The comparison of (a) NH_3 yield and (b) UV-vis absorption spectra of CoS@CN-300, OCP, and Blank were testing at -0.35 V *vs*. RHE.

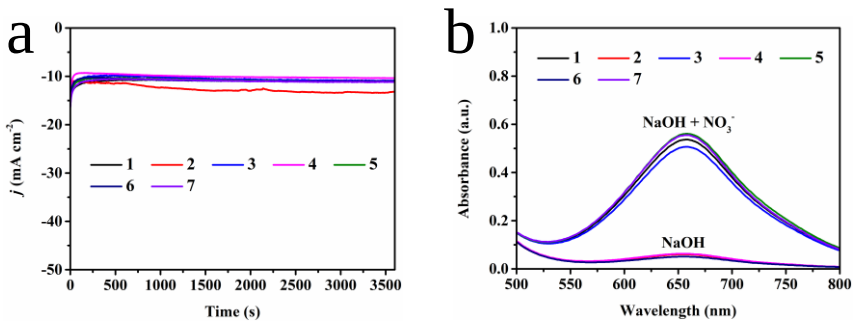

Supplementary Figure 12. The current density and UV-vis absorption spectra of seven alternating cycle tests were accomplished at -0.35 V *vs*. RHE.

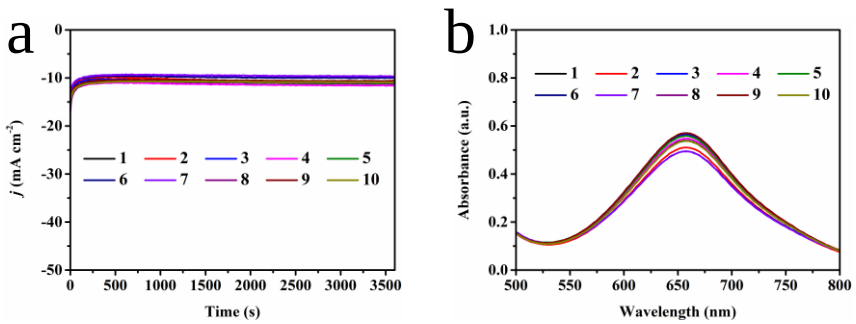

Supplementary Figure 13. The current density and UV-vis absorption spectra of ten cycle tests were accomplished at -0.35 V *vs*. RHE.

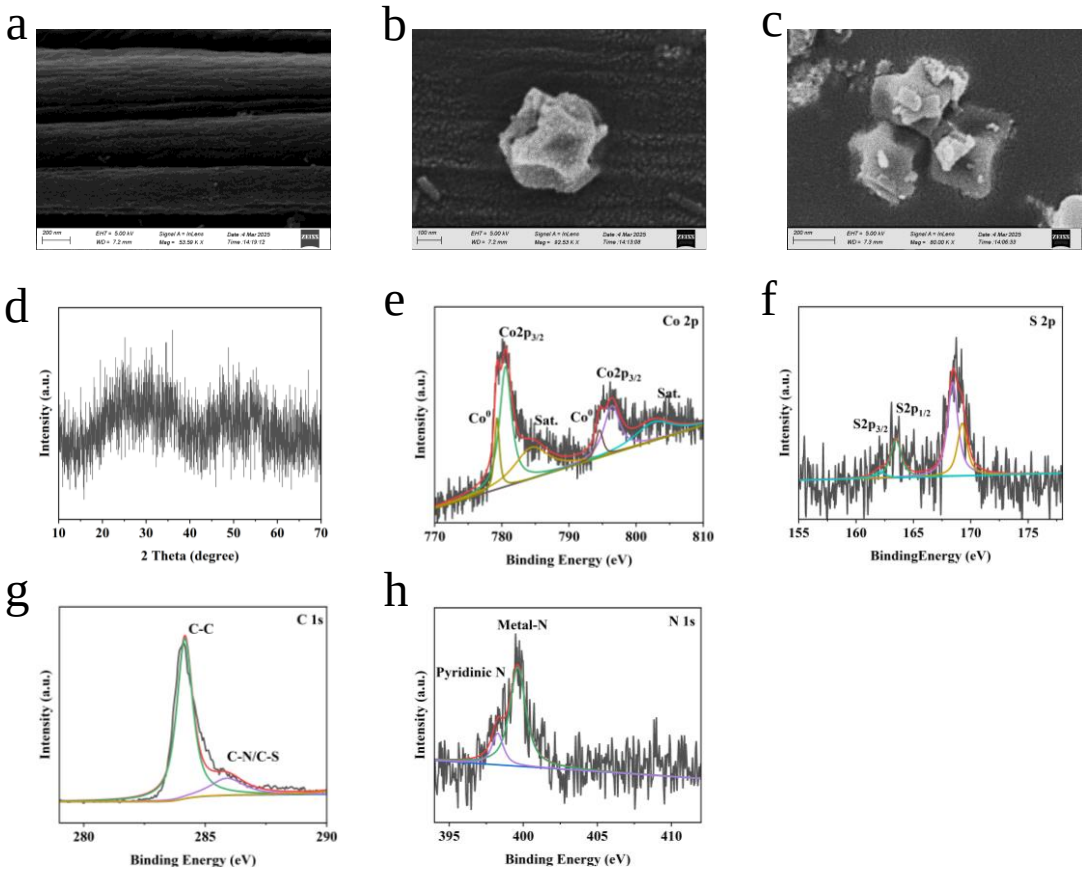

Supplementary Figure 14. SEM (a-c) images of carbon paper and CoS@CN-300, XRD (d) pattern of CoS@CN-300, and XPS (e-h) after eNO_3RR tests.

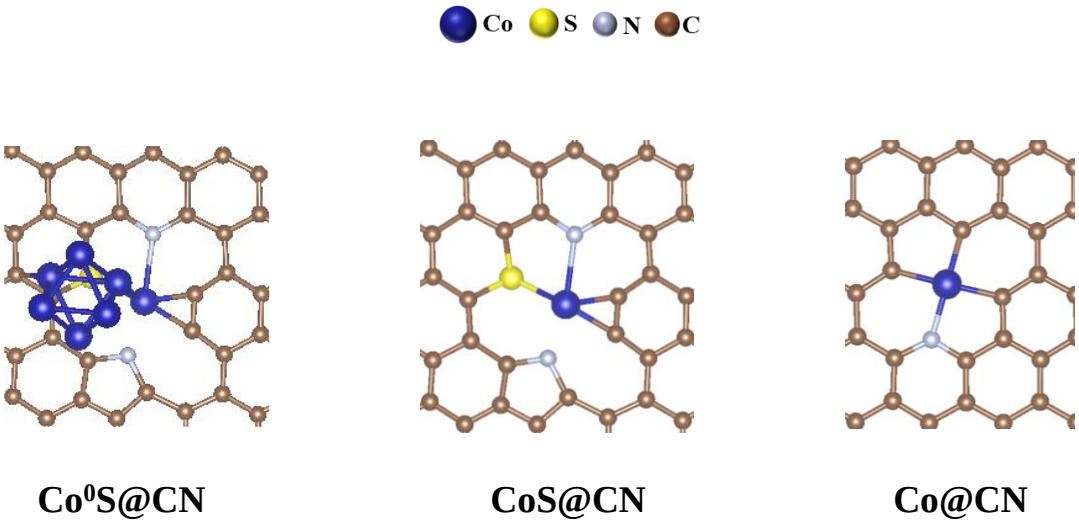

Supplementary Figure 15. The structure of Co^0S@CN, CoS@CN and Co@CN.

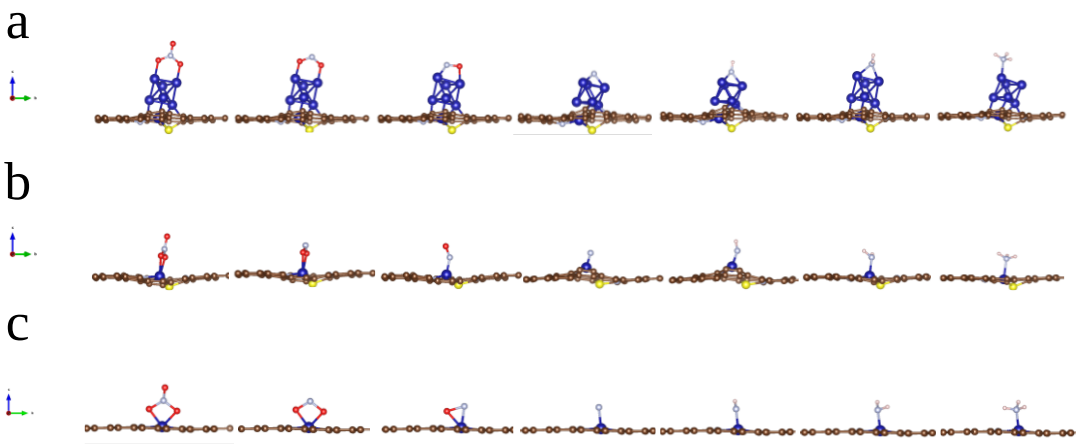

Supplementary Figure 16. The process of NO_3RR on (a) Co^0S@CN, (b) CoS@CN and (c) Co@CN.

Table S1. Comparison of catalytic performances for CoS@CN-300 with other reported eNO_3RR electrocatalysts.

Sample	Specific surface area ($m^2\ g^{-1}$)	Average pore diameter (nm)	Pore volume ($cm^3\ g^{-1}$)
Co@CN-300	1243.48	2.37	0.73
CoS@CN-300	115.83	14.25	0.41

Table S2. Comparison of catalytic performances for CoS@CN-300 with other reported eNO_3RR electrocatalysts.

Catalyst	Electrolyte	Highest FE @ potential	Highest NH_3 Yield rate @ potential	Ref.
CoS@CN-300	0.1 M NaOH with 200 ppm NO_3^-	97.88% @ -0.35 V vs. RHE	4.74 mg h^{-1} mg_{cat}^{-1} @ -0.75 V vs. RHE	This work
CoS@CN-300	0.1 M NaOH with 200 ppm NO_3^-	97.88% @ -0.35 V vs. RHE	80.58 mmol mg h^{-1} cm^{-2} @ -0.75 V vs. RHE	This work
Pb/BC2N	0.1 M KOH with 250 mM NO_3^-	97.42%@ -0.3 V vs. RHE	1.73 mg h^{-1} cm^{-2} @ -0.75 V vs. RHE	[1]
$FeCo_2O_4$	0.1 M KOH with 20 mM NO_3^-	95.9% @ -0.5 V vs. RHE	4.988 mg h^{-1} mg_{cat}^{-1} @ -0.5 V vs. RHE	[2]
$ZnCo_2O_4$	0.1 M Na_2SO_4 with 100 ppm NO_3^-	*	2.1 mg h^{-1} mg_{cat}^{-1} @ -0.64 V vs. RHE	[3]
Cu@NF	1 M KOH with 200 ppm NO_3^-	96.6% @ -0.23 V vs. RHE	0.252 mmol h^{-1} cm^{-2} @ -0.23 V vs. RHE	[4]
Ru@C3N4/Cu	0.1 M KOH with 1400 ppm NO_3^-	91.3% @ -0.8 V vs. RHE	0.249 mmol h^{-1} cm^{-2} @ -0.9 V vs. RHE	[5]
Co_3O_4/Co	0.1 M NaOH with 1000 ppm NO_3^-	88.7% @ -0.8 V vs. RHE	260.5 μmol h^{-1} cm^{-2} @ -0.8 V vs. RHE	[6]
O-Cu-PTCDA	0.1 M NaOH with 500 ppm NO_3^-	85.9% @ -0.4 V vs. RHE	25.65 μmol h^{-1} cm^{-2} @ -0.4 V vs. RHE	[7]
$NiFe_2O_4$/CC	0.1 M PBS with 0.1 M NO_3^-	96.6% @ -0.6 V vs. RHE	623.5 μmol h^{-1} cm^{-2} @ -1.0 V vs. RHE	[8]
CoFeLDH	0.1 M KOH with 1400 ppm NO_3^-	97.68% @ -0.45 V vs. RHE	0.93 mmol h^{-1} cm^{-2} @ -0.45 V vs. RHE	[9]
Co-P/TP	0.2 M Na_2SO_4 with 200 ppm NO_3	95.9% @ -0.3 V vs. RHE	24.47±0.42 μmol h^{-1} cm^{-2} @ -0.6 V vs. RHE	[10]

Reference

[1] X. Li, X. Zhao, Y. Zhou, J. Hu, H. Zhang, X. Hu, G. Hu, Pd nanocrystals embedded in BC2N for efficient electrochemical conversion of nitrate to ammonia, Applied Surface Science 584 (2022) 152556. https://doi.org/10.1016/j.apsusc.2022.152556.

[2] J. Li, D. Zhao, L. Zhang, L. Yue, Y. Luo, Q. Liu, N. Li, A.A. Alshehri, M.S. Hamdy, Q. Lib, X. Suna, A $FeCo_2O_4$ nanowire array enabled electrochemical nitrate conversion to ammonia, Chem Commun (Camb) 58(28) (2022) 4480-4483. https://doi.org/10.1039/d2cc00189f.

[3] P. Huang, T. Fan, X. Ma, J. Zhang, Y. Zhang, Z. Chen, X. Yi, 3D Flower-Like Zinc Cobaltite for Electrocatalytic Reduction of Nitrate to Ammonia under Ambient Conditions, ChemSusChem 15(4) (2022) e202102049. https://doi.org/10.1002/cssc.202102049.

[4] J. Li, J. Gao, T. Feng, H. Zhang, D. Liu, C. Zhang, S. Huang, C. Wang, F. Du, C. Li, C. Guo, Effect of supporting matrixes on performance of copper catalysts in electrochemical nitrate reduction to ammonia, Journal of Power Sources 511 (2021) 230463. https://doi.org/10.1016/j.jpowsour.2021.230463.

[5] Y. Zheng, M. Qin, X. Yu, H. Yao, W. Zhang, G. Xie, X. Guo, Constructing Ru@C(3) N(4) /Cu Tandem Electrocatalyst with Dual-Active Sites for Enhanced Nitrate Electroreduction to Ammonia, Small (2023) e2302266. https://doi.org/10.1002/smll.202302266.

[6] F. Zhao, G. Hai, X. Li, Z. Jiang, H. Wang, Enhanced electrocatalytic nitrate reduction to ammonia on cobalt oxide nanosheets via multiscale defect modulation, Chemical Engineering Journal 461 (2023) 141960. https://doi.org/10.1016/j.cej.2023.141960.

[7] G.F. Chen, Y. Yuan, H. Jiang, S.Y. Ren, H. Wang, Electrochemical reduction of nitrate to ammonia via direct eight-electron transfer using a copper–molecular solid catalyst, Nature Energy 5(8) (2020) 1-9.

[8] L. Xie, L. Hu, Q. Liu, S. Sun, L. Zhang, D. Zhao, Q. Liu, J. Chen, J. Li, L. Ouyang, A.A. Alshehri, Q. Kong, X. Sun, High-performance electrochemical nitrate reduction to ammonia under ambient conditions using NiFe2O4 nanosheet arrays, Inorganic Chemistry Frontiers 9(14) (2022) 3392-3397. https://doi.org/10.1039/d2qi00827k.

[9] F. Du, J. Li, C. Wang, J. Yao, Z. Tan, Z. Yao, C. Li, C. Guo, Active sites-rich layered double hydroxide for nitrate-to-ammonia production with high selectivity and stability, Chemical Engineering Journal 434 (2022) 134641. https://doi.org/10.1016/j.cej.2022.134641.

[10] Z. Li, G. Wen, J. Liang, T. Li, Y. Luo, Q. Kong, X. Shi, A.M. Asiri, Q. Liu, X. Sun, High-efficiency nitrate electroreduction to ammonia on electrodeposited cobalt-phosphorus alloy film, Chem Commun (Camb) 57(76) (2021) 9720-9723. https://doi.org/10.1039/d1cc02612g.